Energy & Environmental Science

Accepted Manuscript

ROYAL SOCIETY OF CHEMISTRY

www.rsc.org/ees

Journal Name

ARTICLE

Efficient band structure tuning, charge separation, visible-light response in ZrS_2-based van der Waals heterostructures†

Received 00th January 20xx,
Accepted 00th January 20xx

DOI: 10.1039/x0xx00000x

www.rsc.org/

Xirui Zhang,[‡a] Zhaoshun Meng,[‡a] Dewei Rao,[bc] Yunhui Wang,[a] Qi Shi,[a] Yuzhen Liu,[a] Haiping Wu,[a] Kaiming Deng,*[a] Hongyang Liu*[b] and Ruifeng Lu*[a]

As a fast emerging hotspot, van der Waals heterostructure can modify two-dimensional (2D) layered materials with desired properties, thus greatly extending the applications of 2D materials. Via state-of-the-art first-principles calculations, we systematically study four types of van der Waals heterostructures formed by monolayer graphene, h-BN, g-C_3N_4, and polyphenylene on ZrS_2 nanosheet. A direct band gap can be obtained in graphene/ZrS_2 heterostructure, endowing graphene with real ability to be applied in nanoelectronics, whereas van der Waals interaction of graphene significantly broadens optical absorption of ZrS_2. The conduction band and valence band of four heterostructures are contributed by ZrS_2 layer and the other layer respectively, so a good charge separation is achieved. We proposed that the strained h-BN/ZrS_2 and g-C_3N_4/ZrS_2 heterostructures satisfy fundamental aspects for photocatalytic water splitting, with the reduction and oxidation levels well inside their band gaps. By forming heterostructures with ZrS_2, the optical properties of h-BN, g-C_3N_4 and polyphenylene show a remarkable improvement in visible light region. The findings in this work will be of broad interest in van der Waals heterostructure research and in photocatalysis field.

Introduction

In recent decade, two-dimensional (2D) materials have shown extraordinary performances in many fields because of their unique electronic, optical, and mechanical properties. The potential applications of 2D materials include catalysis,[1,23] solar cell,[4] lithium-ion battery,[5-7] supercapacitor,[8-10] and superconductivity.[11,12] Following the graphene tide,[13] a lot of analogues such as hexagonal boron nitride (h-BN), graphitic carbon nitride (g-C_3N_4), polyphenylene network that also named as porous graphene (PG), monolayer transition metal dichalcogenides (TMDs), exhibit a wide range of potential in nanoelectronics and catalysis.[14-18] Owing to the advances made in laboratory, such as tandem molecular intercalation, many kinds of few-layer and single-layer TMDs have been successfully produced in recent years.[19-21] Yet not all single-layer nanosheets are perfect materials for certain purposes. For examples, graphene lacks a band gap while the gap of h-BN is too large for electronic and optical applications.[16] As a widely studied photocatalyst, quantum efficiency of pristine g-C_3N_4 needs continuous improvement due to the high recombination rate of the generated electrons and holes.[22] Moreover, PG is not a good candidate for photocatalyst because it displays a photocatalytic activity only in the range of ultraviolet light.[23,24]

For 2D materials utilized in optical applications, there are a number of strategies to improve the performances such as cluster adsorption[22,25] and doping[26] etc. The binding of noble metal clusters such as Pt and Au enhances the visible light absorption of g-C_3N_4,[27] nevertheless, the high cost of noble metal and environmentally unfriendly inherence of these metal clusters are the main disadvantages. Although doping as a common way to change the electronic and optical properties of materials has been extensively studied, including a theoretical work[24] that B, N-doped PG is expected to enhance visible light absorption, it is hard to achieve well-defined doping, and furthermore, the substitutional impurity would become recombination centers and reduce quantum efficiency of photocatalyst.

Over the past years, van der Waals (vdW) heterostructure has been proposed to modify the properties of 2D materials.[28] A monolayer putting on top of another monolayer or few-layer crystal made a vdW heterostructure. Strong covalent bonds keep in-plane stability of 2D crystals while vdW interaction holds the stack together. As novel 2D materials have been developed continually, more vdW heterostructures with desired properties can be built due to their thermal and

[a]Department of Applied Physics, Nanjing University of Science and Technology, Nanjing 210094, P.R. China. E-mail: rflu@njust.edu.cn; kmdeng@njust.edu.cn; Tel: +86-25-84315882
[b]Shenyang National Laboratory for Materials Science, Institute of Metal Research, Chinese Academy of Sciences, 72 Wenhua Road, Shenyang 110016, P.R. China. E-mail: liuhy@imr.ac.cn; Tel: +86-24-83970027
[c]Institute for Advanced Materials, Jiangsu University, Zhenjiang 212013, P.R. China
[‡]These authors contributed equally to this work.
† Electronic Supplementary Information (ESI) available: [http://]. See DOI: 10.1039/x0xx00000x

chemical stability. More importantly, vdW heterostructure could bring improvements in terms of electronic and optical properties by combining together the advantages of its building monolayers, which have been found experimentally and theoretically, such as a tenfold increase in electronic quality of h-BN/graphene compared to graphene,[29] graphene/g-C_3N_4 bilayer for visible-light response,[30] MoS_2-WS_2 for ultrafast charge transfer,[31] WS_2/rGO vdW heterostructures as catalyst[32] and MoS_2/p-Si for solar cell,[33] and so on.

As a representative TMD, ZrS_2 shows good thermodynamic stability, environmental friendliness, high sensitivity, and low-cost production. With respect to photo response, ZrS_2 nanoribbons have been applied in photodectors[34] and solar cells.[35] In recent years, 2D ZrS_2 monolayer which inherits these advantageous qualities was successfully fabricated by electrochemical lithiation process[36] or by using h-BN as a deposition template[37] or by an effective alternative (tandem intercalation strategy)[38] to conventional exfoliation processes. The conduction band minimum (CBM) of ZrS_2 monolayer is slightly lower than the reduction level of hydrogen, which was excluded in computational screening of potential photocatalysts.[39] The band structure of the ZrS_2 monolayer is remarkably modified when a symmetrical uniform strain is applied to it. In more detail, the band gap of ZrS_2 monolayer can be tuned from 0 to 2.47 eV by –10% ~ 15% strain and its CBM could easily move upon the standard hydrogen electrode potential.[40]

Besides, 2D ZrS_2 nanosheet has a unique feature among TMDs: its lattice parameter is a = 3.68 Å[39] that could closely match with the lattices of many well-known 2D materials. As schematically illustrated in Figure 1, layered ZrS_2 with a 2×2 supercell could pair with most popular 2D materials, such as 3×3 supercells of graphene (a = 2.46 Å),[13] h-BN (a = 2.5 Å),[41] and BC_2N (a = 2.44 Å),[42] unit cells of g-C_3N_4 (a = 7.13 Å)[3] and PG (a = 7.45 Å)[23]. Very small lattice mismatch (Table 1) makes ZrS_2 a suitable substrate for these 2D materials, therefore, ZrS_2 monolayer should be an ideal subassembly of bilayer or multilayer vdW heterostructures.

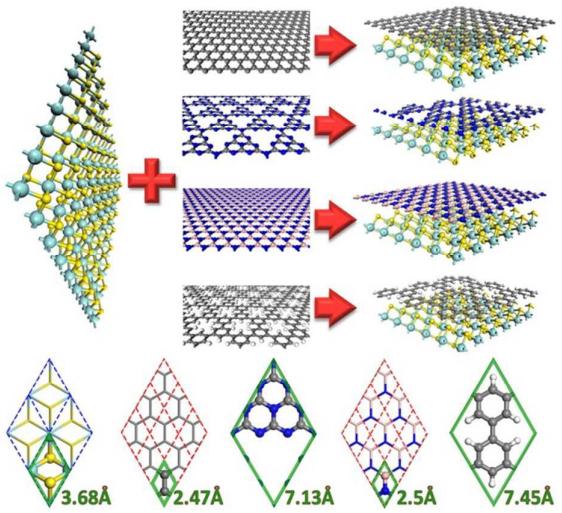

Fig. 1 Schematical diagram for van der Waals heterostructures based on ZrS_2 monolayer. Left: The ZrS_2 monolayer. Middle: From the top down, graphene, g-C_3N_4, h-BN and PG monolayer, Right: The corresponding vdW heterostructures. Bottom: Supercells employed in our calculations with optimized lattice constants of unit cell (in green diamond) of all five monolayers.

Table 1 Geometric parameters and binding energies of vdW heterostructures

Heterostructure	η	R_e (Å) [a]	E_b (eV)
Graphene/ZrS_2	0.7%	3.41	–1.67
h-BN/ZrS_2	1.9%	3.35	–1.63
g-C_3N_4/ZrS_2	–3.1%	3.38	–1.03
PG/ZrS_2	1.2%	3.30	–0.54

[a]Equilibrium distances (R_e) of the optimized vdW heterostructures are the average distance between the S-atom layer of ZrS_2 and the other monolayer.

The main goal of this study is to unveil whether or not the bilayer vdW heterostructures based on ZrS_2 monolayer enhance the visible-light response or improve electronic properties of these 2D materials. We investigated four vdW heterostructures: graphene/ZrS_2, h-BN/ZrS_2, g-C_3N_4/ZrS_2, and PG/ZrS_2, and particular attention will be focused on the following questions: (i) Will a gap be opened in graphene? (ii) Will the band gap and absolute values of conduction band (CB) and valence band (VB) be suitable for water splitting? (iii) Is there charge separation in heterostructures and strong electron coupling at the interface? (iv) Will the optical absorption of these vdW heterostructures be in the visible light region? (v) Does the electronic and optical properties remain unchanged when apply acceptable strains on the heterostructures?

Model and Methods

The geometric model of vdW heterostructures was composed of 2×2 ZrS_2 supercell and 3×3 supercell of graphene, h-BN, unit cell of g-C_3N_4, and PG nanosheets. A vacuum space is set to be 20 Å in order to avoid the interactions between neighboring heterostructures. For convenience, all heterostructure models have the same lattice constants of a=b=7.36Å which corresponds to the optimized 2×2 supercell of ZrS_2 monolayer and all applied strains on heterostructures are based on this lattice parameter.

The lattice mismatches of the supported nanosheets to ZrS_2 monolayer in heterostructures is defined by $\eta = (c_{\text{others}} - c_{ZrS_2}^{2\times2})/c_{ZrS_2}^{2\times2}$, where $c_{ZrS_2}^{2\times2}$ is the optimized lattice parameter of 2×2 ZrS_2 super-cell, c_{others} corresponds to the optimized lattice parameters of 3×3 super-cells of graphene and h-BN, unit cells of g-C_3N_4 and PG, therefore, the calculated mismatches are 0.7%, 1.9%, –3.1%, and 1.2% for graphene, h-BN, g-C_3N_4 and PG (Table 1), respectively, which are all in acceptable range and accessible in experimental synthesis.

The equilibrium distances between two layers are about 3.3~3.4 Å (Table 1) in the optimized graphene/ZrS_2, h-BN/ZrS_2, g-C_3N_4/ZrS_2, and PG/ZrS_2 heterostructures. It should be noted that van de Waals correction of nonbonding interaction is very important for accurately describing the geometries in layered heterostructures. The fluctuation of graphene, h-BN, g-C_3N_4 is very tiny, however, PG has a buckling distance about 1.0 Å for

its H atoms linked by C atoms and seemingly won't be stable to stay in one plane.

The interfacial binding energy (E_b) can be computed according to the equation, $E_b = E_{X/ZrS_2} - (E_X + E_{ZrS_2})$, where E_{X/ZrS_2}, E_X, and E_{ZrS_2} represent the total energy of heterostructures, isolated nanosheets (X = graphene, h-BN, g-C_3N_4, PG), and isolated ZrS_2 monolayer, respectively. The calculated binding energies are –1.67 eV, –1.63 eV, –1.03 eV, and –0.54 eV for graphene/ZrS_2, h-BN/ZrS_2, g-C_3N_4/ZrS_2, and PG/ZrS_2 heterostructures (Table 1), respectively, which imply their high stability under normal conditions.

All the density functional theory calculations were performed using the Vienna Ab-initio Simulation Package (VASP) code.[43-45] Generalized gradient approximation in the parametrization of Perdew-Burke-Ernzerhof (PBE)[44] and the vdW correction proposed by Grimme are chosen.[46] The energy cutoff was set to be 550 eV. Geometry structures are fully relaxed until the convergence criteria of energy and force are less than 10^{-5} eV and 0.01 eV Å^{-1}, respectively. A Monkhorst-Pack mesh of 7×7×1 k-points is used in the 2D Brillouin zone for geometry optimizations and electronic structure calculations. We also used a large vacuum space to calculate the absolute position of the band dispersion for quantitatively comparing with the standard hydrogen electrode potential. Since the calculated vacuum level by averaging the LOCPOT file along the specified plane from VASP is a relative value, we shifted the band structure by subtracting this value to obtain the absolute band edge position. Importantly, because the PBE functional underestimates the band gaps of semiconductors, all electronic structures and optical absorption coefficients were further calculated using the HSE06 hybrid function.[47]

Results and Discussion

The graphene/ZrS_2 heterostructure

The lattice constants of graphene and ZrS_2 monolayers are calculated to be 2.47 Å and 3.68 Å, respectively, in good agreement with previous study.[13,48] It should be noted that it is the K point of the Brillouin zone where the Dirac cone is in the graphene primitive cell. However, due to the band folding, Dirac cone is at the Γ point of the Brillouin zone of the 3 × 3 supercell.[49] For 2×2 ZrS_2 supercell, the CBM and valence band maxinum (VBM) are both located at Γ point of the Brillouin zone. In our calculations, 2×2 ZrS_2 supercell has a direct band gap of 1.11 eV from PBE and 1.94 eV from HSE06. Such a difference clearly verifies the importance of using the hybrid functional to obtain an accurate band gap. The gapless characteristic remains in a 3×3 graphene supercell, although this 3×3 supercell has been actually applied by a 0.7% strain so as to fit the 2×2 ZrS_2 supercell.

The band structure of the graphene/ZrS_2 heterostructure calculated by HSE06 hybrid functional is shown in Fig. 2a, from which we can see that there is a "half" Dirac cone at the Γ point of the Brillouin zone, which has a VB part same with the VB of graphene and a smooth CB part. Close examination reveals a 70 meV direct band gap which is shown in the enlarged inset in Fig. 2a around the Γ point. It is interesting that the shape of CB in graphene/ZrS_2 heterostructure is totally different from the CB of graphene. To address the CB changing and explore more details of the electronic structures,

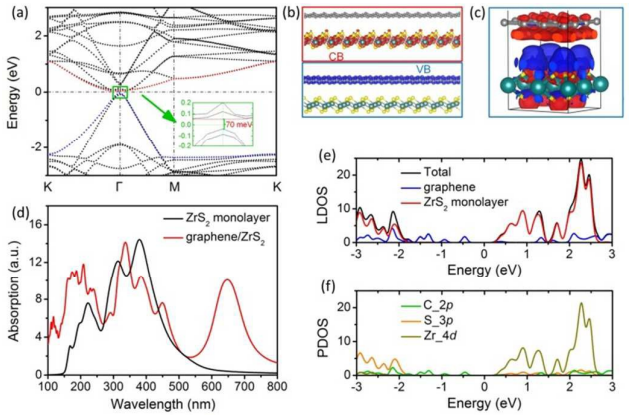

Fig. 2 Electronic and optical properties of graphene/ZrS_2 heterostructure. (a) Calculated band structure of graphene/ZrS_2 heterostructure. Inset is magnification of the bands near the Γ point showing the band gap opening. (b) The charge densities of the VB (blue) and CB (red) for graphenen/ZrS_2 with an isovalue of 0.04 e/Å^3. (c) Charge density differences of hybrid graphene/ZrS_2 heterostructure compared with the isolated ZrS_2 and graphene monolayers. Grey, yellow, and dark green balls represent C, S and Zr atoms, respectively. Blue and red isosurfaces represent, respectively, charge accumulation and depletion. The isovalue chosen to plot the isosurfaces is 0.002 e/Å^3. (d) Calculated light absorption properties of graphene/ZrS_2 heterostructure and ZrS_2 monolayer. Calculated local DOS (e) and partial DOS (f) of graphene/ZrS_2 heterostructure. The Fermi level is set to zero for clarity.

local density of states (DOS) and partial DOS are displayed in Fig. 2e and 2f, from which we can draw a conclusion that the CB of graphene/ZrS_2 heterostructure is contributed by Zr_4d orbital while the VB is contributed by C_2p orbital. To confirm this, we also calculated the charge densities of CB and VB, in Fig. 2b, and there is no doubt that the charge density of CB distributes around the Zr atoms while that of VB is exactly around C atoms.

Furthermore, we observe a charge redistribution which mainly occurs at the interface region in the charge density differences of hybrid graphene/ZrS_2 heterostructure compared with the free ZrS_2 and graphene monolayers in Fig. 2c. Although the obvious charge separation between the graphene and ZrS_2 sheet will result in weak donor–acceptor coupling, there is still certain charge transfer from graphene to ZrS_2.

Similar to the explanation regarding the gap opening of graphene/g-C_3N_4 heterostructure,[31] the ZrS_2 substrate generates inhomogeneity in the graphene electrostatic potential over the graphene layer, which changes the potential periodicity of graphene and thus breaks the degeneracy of the π and π* bands at the Γ point, resulting in a 70 meV gap and a "half" Dirac cone. The photoexcited e^- and h^+ carriers of this heterostructure are well separated that the hole will move inside the graphene layer and the electron will move inside the ZrS_2 layer. We note that the calculated room-temperature electron mobility[50] of ZrS_2 monolayer is much higher than that of MoS_2 but much lower than the unprecedented high carrier mobility of graphene.[51] In graphene/ZrS_2 heterostructure, the recombination of carriers will be reduced with an improved quantum efficiency for optoelectronics applications, due to not only the efficient charge separation but also the large difference between the hole mobility from the "half" Dirac core and the electron mobility from the CB contributed by Zr atoms.

As mentioned above, strain can tune the band structures of ZrS_2 monolayer, which creates a probability to further open the band gap of graphene/ZrS_2 heterostructure. A larger 120 meV direct band gap can be obtained when 3% strain is applied on the heterostructure. In previous work, applying 5% isotropic strain on graphene only gives a direct band gap of about 10 meV.[52] The remarkable enlargement of band gap by strain on graphene/ZrS_2 heterostructure is closely connected to the separation of charge densities of CBM and VBM. With a 70 or 120 meV direct band gap that is significantly larger than the room-temperature thermal energy (k_BT), graphene/ZrS_2 heterostructure is promising for nanoelectronics application such as field effect transistor, because the "half" Dirac cone remains the relatively high electron mobility of ZrS_2 and the extremely high hole mobility of graphene.

In addition to an effective peak value around wavelength of 650 nm, the light absorption property of graphene/ZrS_2 shows a wide range of visible light response, which may have advantage in both visible light generation and harvesting (Fig. 2d). It should be noticed that the strong electron coupling at the graphene/ZrS_2 interface may induce a unique optical transition. As shown in the band structure of the hybrid graphene/ZrS_2 heterostructure (Fig. 2a), electrons would be directly excited from the VB of graphene to the CB of ZrS_2. This may conduce to the application of graphene in photodetection and photoconductivity applications benefiting from its high hole mobility, low recombination rate, and small band gap.[30,53]

The h-BN /ZrS_2 heterostructure

Hexagonal boron nitride sheet is analogous to graphene in structure but they are very different in terms of other properties.[16,18] In 2004, Corso et al.[42] successfully produced h-BN nanomesh on Rh(111) single crystalline surface by selfassembly and in the following year Novoselov et al.[54] reported free standing h-BN crystallites using mechanical cleavage. Afterwards, h-BN has motivated tremendous amounts of theoretical and experimental investigations and many advanced technologies are based on it. Monolayer h-BN has a large band gap of 4.5 eV. Its popular name "white graphene" means very weak visible light response. Experimentally, a hybrid h-BN/ZrS_2 nanocomposite has been already synthesized which exhibits an n-type transport behavior.[37] So far its optical absorption properties remain unexplored. There are many studies reported that constituting a hybrid nanocomposite could promote optical performance of materials, which is expected workable for h-BN/ZrS_2 heterostructure.

The calculated optical absorption spectra of the h-BN monolayer, the hybrid h-BN/ZrS_2 heterostructure, and the h-BN/ZrS_2 heterostructure with 3% strain are plotted in Fig. 3b. Compared with the pure h-BN, the optical absorption property of h-BN/ZrS_2 heterostructure shows a great improvement. The optical absorption edge of h-BN/ZrS_2 heterostructure increases to about 550 nm while that of h-BN is at 130 nm. And the absorption region above 400 nm is clearly enhanced in h-BN/ZrS_2 heterostructure. This edge and one of the main absorption shoulders of h-BN/ZrS_2 heterostructure are in typical visible region. Around 450 nm where is the top of solar energy distribution, the absorption of h-BN/ZrS_2 vdW heterostructure is still dominant with a considerable absorption intensity.

The band gap of h-BN/ZrS_2 heterostructure is calculated to be 1.56 eV which is much smaller than that of pure h-BN monolayer. The VBM and CBM of h-BN/ZrS_2 are both at the Γ point and come from h-BN and ZrS_2, respectively. By comparing the band structures of graphene/ZrS_2 and h-BN/ZrS_2, it is obvious that the CBs of them are similar. It is verified by their partial DOSs (Fig. 3d) that the CB of h-BN/ZrS_2 vdW heterostructure is contributed by Zr_4d orbitals while the VB is contributed by atoms of the other layer such as N atoms in h-BN layer. The local DOS reveals that the CB and VB of h-BN/ZrS_2 are separately from two layers, and the charge separation is also apparent from charge density plot (Fig. 3c). The charge density of CB in heterostructure distributes around Zr atoms in ZrS_2 layer while charge density of VB distributes among the other layer (h-BN). We know that the recombination of photon-generated carriers is a dominant factor of the low quantum efficiency for most photocatalysts. A good separation of e^--h^+ couples would vastly reduce the recombination. The charge distribution of h-BN/ZrS_2 heterostructure shows a very good charge separation. The distribution center of hole is mainly around Zr atom whereas the electron density is distributed around N atom. The distance between Zr and N atoms is large at about 4.76 Å. As found in previous studies and in present work, there is no visible light absorption in pure h-BN (Fig. 3b), while there is no efficient charge separation in pure ZrS_2 monolayer (Fig. S1†). However, h-BN/ZrS_2 heterostructure efficiently achieves charge spatial separation into two layers while keeps the advantage of good visible light absorption of ZrS_2.

To successfully produce H_2 and O_2 during water splitting using h-BN/ZrS_2 heterostructure as a photocatalyst, the reduction and oxidation levels which are respectively –4.44 eV for H^+ to H_2 and –5.67 eV of H_2O to O_2, should be both located inside the band gap of h-BN/ZrS_2. It has been claimed that band edge positions of isolated ZrS_2 monolayer are not suitable for photocatalytic splitting of water, for its CBM is slightly lower than the reduction level by 0.14 eV,[39] and the CBM of h-BN/ZrS_2 heterostructure is 0.07 eV lower than –4.44

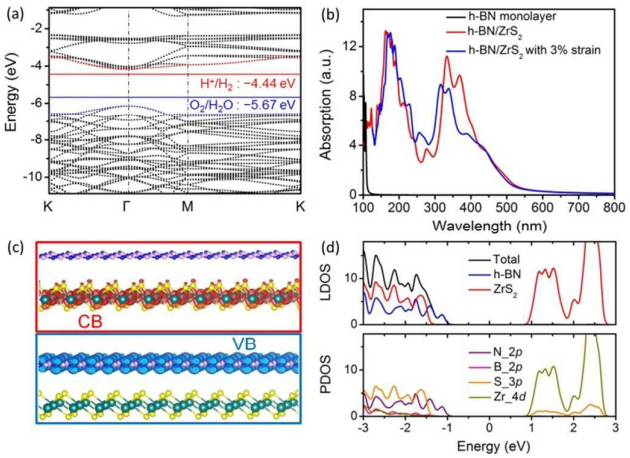

Fig. 3 Electronic and optical properties of h-BN/ ZrS_2 heterostructure. (a) Calculated band structure with respect to the vacuum level for h-BN/ZrS_2 heterostructure by applying 3% strain. The position of the reduction level for H^+ to H_2 is indicated by the red line and the oxidation potential of H_2O to O_2 is in blue line. (b) Calculated light absorption properties of h-BN monolayer, h-BN/ZrS_2 heterostructure, and h-BN/ZrS_2 heterostructure by applying 3% strain. (c) The charge densities of the VB (blue) and CB (red) for h-BN/ZrS_2 with an isovalue of 0.02 e/Å^3. (d) Calculated local DOS and partial DOS of h-BN/ZrS_2 heterostructure.

eV in our calculation. However, the CBM of ZrS_2 monolayer can be elevated by applying strains. When a 3% biaxial strain is applied on the h-BN/ZrS_2 heterostructure, the CBM at the Γ point moves up by 0.32 eV and then becomes 0.25 eV higher than the reduction level of H_2O, rendering h-BN/ZrS_2 able to produce H_2 and O_2 at the same time (Fig. 3a). A higher CBM with a larger driving force for electron transfer can be accomplished if applying a larger strain on h-BN/ZrS_2. We also examine the strain effect on optical property of h-BN/ZrS_2 heterostructure, the first peak in the range of visible light is blue shifted only by 30 nm. Also, the absorption intensity at the dominant wavelength (400~500 nm) of solar light is unchanged, as shown in Fig. 3b. With low cost, high thermal stability, fascinating charge separation, efficient visible light absorption, and well-positioned band edge, h-BN/ZrS_2 heterostructure is a very promising material in photovoltaic and photocatalytic applicatons.

The g-C_3N_4/ZrS_2 heterostructure

As one of the oldest synthetic polymers since Liebig first reported melon structure in 1834,[55] different kinds of polymeric carbon nitrides have been synthesized in many laboratories due to the widespread applications in traditional catalysis and photocatalysis. Wang et al.[1,3] have reported that polymeric carbon nitride is able to generate hydrogen from water in the absence of noble metals, nevertheless, there is a lack of light absorption above 390 nm. Most recently, Liu et al.[2] shifted the optical absorption of C_3N_4 to the visible range by designing a stable carbon nanodot–carbon nitride nanocomposite (CDots-C_3N_4), and the measured quantum efficiencies for photocatalytic water splitting are prominently improved around 420 nm and even extending to 600 nm. Many other strategies have also been presented to improve the photocatalytic ability of g-C_3N_4,[56] such as fabrication of nano/mesoporous structures,[3,57] noble metal modification.[22,27] The expensive cost of noble metals will hinder the practical application of g-C_3N_4 as a photocatalyst, whereas fabrication of vdW heterostructure by different nanosheet is a striking way,[27,58-63] because the formed nanocomposite not only reduces the recombination of photo-excited electrons and holes but also ameliorate other properties such as band structure and optical absorption.[3,30,57,61,64]

In pursuing an appropriate material for vdW heterostructure with g-C_3N_4, Hou et al. significantly improved the H_2 production performance of g-C_3N_4 under visible light by growing thin layers of MoS_2 on g-C_3N_4.[61] The mechanism was explored by Wang et al.[65] using a type of g-C_3N_4 with a small pore. The lattice constant of experimentally available g-C_3N_4 with larger pores is 7.13 Å and the lattice constant of MoS_2 is 3.19 Å. The large lattice mismatch means a big challenge to realize nanocomposites based on MoS_2 and large-pore g-C_3N_4. Fortunately, as suggested in abovementioned section, ZrS_2 is the ideal substrate for large-pore g-C_3N_4 to form vdW heterostructure.

In present work, the optimized lattice constant of the large-pore g-C_3N_4 monolayer is 7.13 Å, the band gap is 2.7 eV, and the peak of optical absorption coefficient is at about 270 nm that corresponds to a UV light. These properties are in good agreements with previous works.[30] The CBM of g-C_3N_4 monolayer is higher than the reduction level of hydrogen by 1.2 eV which generates a high driving force to product H_2 without the help of cocatalysts. However, on account of the

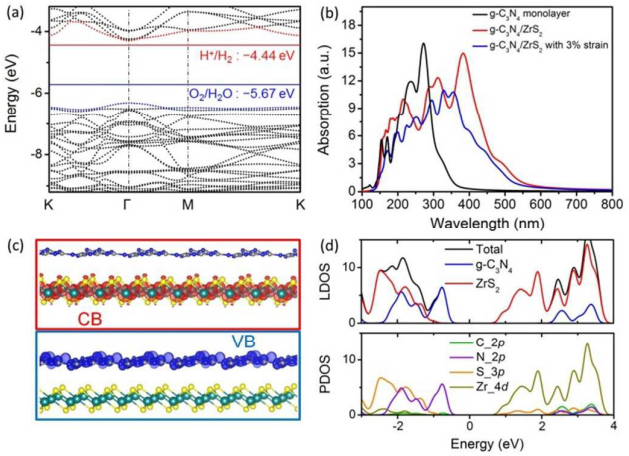

Fig. 4 Electronic and optical properties of g-C_3N_4/ZrS_2 heterostructure. (a) Calculated band structure with respect to the vacuum level for g-C_3N_4/ZrS_2 heterostructure by applying 3% strain. The position of the reduction level for H^+ to H_2 is indicated by the red line and the oxidation potential of H_2O to O_2 is in blue line. (b) Calculated light absorption properties of g-C_3N_4 monolayer, g-C_3N_4/ZrS_2 heterostructure and g-C_3N_4/ZrS_2 heterostructure by applying 3% strain. (c) The charge densities of the VB (blue) and CB (red) for g-C_3N_4/ZrS_2 with an isovalue of 0.02 e/Å^3. (d) Calculated local DOS and partial DOS of g-C_3N_4/ZrS_2 heterostructure.

short distance between e^- and h^+ charge distribution in the same plane of g-C_3N_4, the high recombination rate of e^--h^+ pairs will cause a low water splitting rate.

The charge distribution of g-C_3N_4/ZrS_2 vdW heterostructure (Fig. 4c) shows a very good charge separation. The e^- charge distribution center is mainly around Zr and the h^+ charge distribution is around N. There is a large distance of about 4.7 Å between Zr and N atoms. So the present of ZrS_2 will bring an improvement of the photocatalysis performance of g-C_3N_4 in e^--h^+ separation. We also find a charge redistribution which mainly occurs at the interface region in the charge density differences of hybrid g-C_3N_4/ZrS_2 heterostructure compared with the freestanding ZrS_2 and g-C_3N_4 monolayers (Fig. S3†). The internal polarized field is considered as a source of photocatalyst performance enhancement, similar to the g-C_3N_4/graphene heterostructure[30] and g-C_3N_4/MoS_2 heterostructures.[65]

The band gap of g-C_3N_4/ZrS_2 calculated by HSE06 hybrid function was 1.71 eV which is clearly larger than the theoretic limit value of 1.23 eV for water splitting. It should be noticed that the nanocomposite's VBM is at Γ point similar to g-C_3N_4 monolayer and the nanocomposite's CBM is at Γ point similar to ZrS_2 monolayer. From the DOS analyses, the VB of g-C_3N_4/ZrS_2 is mostly contributed by N_2p orbital of g-C_3N_4 while the CB of g-C_3N_4/ZrS_2 is mostly contributed by Zr_4d orbital of ZrS_2 (Fig. 4d). In order to match the reduction and oxidation levels of H_2O, we apply 3% strain on the g-C_3N_4/ZrS_2 heterostructure. The strained g-C_3N_4/ZrS_2 heterostructure has a direct band gap of 2 eV at Γ point of the Brillouin zone (Fig. 4a). The CBM is 0.2 eV higher than the reduction level and the VBM is 0.6 eV lower than the oxidation level of H_2O to O_2, which guarantee the driving forces for both electron and hole transfer in H_2 and O_2 evolutions.

The calculated optical absorption spectra of the g-C_3N_4 monolayer, the strained and unstrained g-C_3N_4/ZrS_2 heterostructures are plotted in Fig. 4b. The optical absorption

edge of g-C_3N_4/ZrS_2 heterostructure increases to about 550 nm compared to 350 nm of g-C_3N_4 monolayer. Also, the main peak moves from 270 nm of g-C_3N_4 to 390 nm of hybrid g-C_3N_4/ZrS_2 heterostructure. For both 3%-strained and unstrained g-C_3N_4/ZrS_2 heterostructures, the dominant absorption area almost has a double expansion. It clearly shows that g-C_3N_4/ZrS_2 heterostructure remains the good visible light absorption of ZrS_2 monolayer (Fig. 2b), therefore, g-C_3N_4/ZrS_2 can be suggested as a promising photocatalyst. As well expounded in a recent review,[1] g-C_3N_4 and kinds of face-to-face contacted nanocomposites containing g-C_3N_4 have robust stability against photocorrosion. Also, stability of g-C_3N_4/MoS_2 van der Waals heterostructure has been proved experimentally.[61] Analogously, the g-C_3N_4/ZrS_2 should be also stable under light irradiation and mild chemical conditions for their binding energies are close.

The PG/ZrS_2 heterostructure

In experiments, a recently synthesized 2D polyphenylene network, also known as porous graphene,[66,67] has been demonstrated to possess semiconductor characteristics with a gapped band structure. Based on PG structure, multifunctional properties have been widely studied, including applications for gas adsorption and separation.[68,69] HSE06 hybrid functional calculations[23] show that a direct band gap of 3.2 eV corresponding to the ultraviolet absorption region, which is still large for necessitating visible-light absorption. Although previous theoretical work designed a hybrid nanosheet by doping B and N in PG to meet all fundamental requirements for photocatalytic water splitting,[24] that perfect doping is very difficult to achieve in laboratory. Thus, the question is how to enhance the visible-light absorption of PG in a more practical way. Here, we seek for the help of vdW heterostructure.

Like graphene, h-BN and g-C_3N_4 in previous sections, we place a PG unit cell on the 2×2 ZrS_2 supercell, and the lattice mismatch of 1.2% between PG and ZrS_2 is small and still achievable in experiment. After relaxation of the PG/ZrS_2 heterostructure, the light H atoms of C-H bonds located at pores in original PG move out of PG plane due to the interaction with ZrS_2 layer. The fluctuation of PG in the vdW heterostructure is about 0.97 Å and much obvious than other heterostructures. Moreover, the interlayer distance between PG and ZrS_2 layers is about 3.3 Å, which is a little smaller than those of other heterostructures. The binding energy for PG/ZrS_2 is the smallest one among four heterostructures (see Table 1) which is understandable due to only two aromatic rings interacting with ZrS_2 layer, nevertheless, PG/ZrS_2 would be still stable at moderate temperature.

The calculated optical absorption spectrum of PG/ZrS_2 heterostructure is presented in Fig. 5b. The main peak of the PG is at 280 nm, exhibiting a clear ultraviolet absorption. The weak visible-light activity of the pristine PG indicates no much prospect for a solar absorber. Surprisedly, the calculated optical absorption property of the PG/ZrS_2 has a peak at 380 nm, redshifting obviously by 100 nm and the absorption edge is at about 550 nm. The optical absorption of PG is greatly enhanced in the visible region of the solar spectrum by forming a PG/ZrS_2 heterostructure.

This can be understood by the band structure of PG/ZrS_2 heterostructure in Fig. 5a which shows an indirect band gap of 1.03 eV. The CBM is at Γ point and the VBM is at K point of the Brillouin zone. With the value smaller than 1.23 eV, the band gap of PG/ZrS_2 heterostructure could not span over both reduction energy level of H_2 and oxidation energy level of H_2O to O_2. With respect to the vacuum level, we calculated the absolute positions of CBM and VBM and find that only the oxidation energy level of H_2O to O_2 is between them. The reduction level for H^+ to H_2 is above the CBM by 0.7 eV, obviously outside the band gap, thus acceptable strain on PG/ZrS_2 heterostructure is hard to lower it much down.

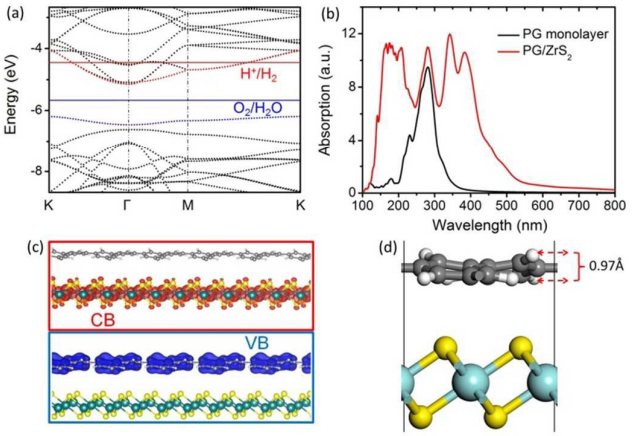

Fig. 5 Electronic and optical properties of PG/ZrS_2 heterostructure. (a) Calculated band structure with respect to the vacuum level for PG/ZrS_2 heterostructure. The position of the reduction level for H^+ to H_2 is indicated by the red line and the oxidation potential of H_2O to O_2 is in blue line. (b) Calculated light absorption properties of PG monolayer and PG/ZrS_2 heterostructure. (c) The charge densities of the VB (blue) and CB (red) for PG/ZrS_2 with an isovalue of 0.02 e/Å^3. (d) Structural details of PG/ZrS_2 heterostructure, where PG layer shows a fluctuation of 0.97 Å.

Same with other three heterostructures under study, PG/ZrS_2 heterostructure has a good separation in electron and hole distribution (Fig. 5c). The VB is contributed by the 4d orbital of Zr atom and the CB comes from the 2p orbital of C atom of the PG layer. The distance between e^- and h^+ charge distribution centers is also remarkably large of 4.5 Å. Compared with the original PG, e^--h^+ separation would reduce the recombination of photon-generated carriers and ensure its quantum efficiency. The results of band structure, optical absorption, and charge distribution endue PG/ZrS_2 heterostructure with a wonderful capacity of O_2 evolution from water splitting under visible light if an appropriate electron scavenger presents.

Conclusions

In summary, we designed four vdW heterostructures based on ZrS_2 monolayer and theoretically studied their structural, electronic and optical properties. Intensive hybrid functional calculations by using the HSE06 functional and by including long-range dispersion corrections have been carried out. The chosen graphene, h-BN, g-C_3N_4, polyphenylene, and ZrS_2 monolayers are all available under current experimental conditions. Since most of the solar energy comes from the visible-light region, to enhance the quantum efficiency, the absorption peak of photovoltaic cells and photocatalytic materials should be located within the range from 400 nm to 760 nm. Our results show that good visible light response was found in all four vdW heterostructures.

The band gap of graphene is opened through the vdW

interaction of the ZrS_2 monolayer, and strain on graphene/ZrS_2 heterostructure can open a relatively large gap to be practically applied in future semiconductor industry. From our calculations, the CBs are contributed by ZrS_2 layer and the VBs are contributed by the other layer in all four heterostructures. Thus, lowered band gap (except for graphene/ZrS_2) and good charge separation are achieved. The charge accumulation/depletion at the interfaces is generated by the type II band alignment. By forming the layered heterojunction, the charge accumulation/depletion at the interfaces is generated by the type II band alignment, so the photogenerated electrons move from other layer to ZrS_2, while the photogenerated holes would transfer from ZrS_2 to the other layer by the VB offset, both of which will facilitate the exciton dissociation. Moreover, the charge diffusion distance is reduced from the bulk to the surface, and thus reducing the recombination possibility during the migration. For photocatalytic water splitting, h-BN/ZrS_2 and g-C_3N_4/ZrS_2 heterostructures can meet three fundamental requirements, i.e., suitable CBM and VBM positions with enough driving forces for electron and hole transfer, efficient charge separation, and good optical absorption under visible light. For polyphenylene/ZrS_2 heterostructure, only the oxidation level of H_2O to O_2 is inside the band gap, and the visible light absorption benefits from the good optical response of ZrS_2 monolayer, so polyphenylene/ZrS_2 could be a hopeful photocatalyst for O_2 production if an electron scavenger is introduced.

The findings in this article have properly answered the five questions put forward in the introduction section, and we demonstrate again that vdW heterostructures should be paid more attentions in future experiments, especially emphasizing the ZrS_2-based heterostructures due to their tunable band structure, good charge separation, and promising visible-light response, and inspiritingly, the synthesis of ZrS_2 monolayer is no longer a big challenge with the development of experimental techniques,[35-38] although it was initially excluded in computational screening of potential photocatalysts.[39] Further, as reviewed in a perspective by Geim and Grigorieva,[28] there would be unlimited possibility of fabricating vdW heterostructures with the discovery of more and more 2D materials including graphene family, 2D chalcogenldes, 2D oxides, etc. At least, beyond the four ZrS_2-based heterostructures under study, fluorographene, graphene oxide, ternary BCN,[70] chemically-functionalized g-C_3N_4 , and other TMDs like MoS_2 could be utilized to assemble bilayer or even multilayer Lego-like structures for particular or multifunctional applications, which should be studied soon by our own or by other researchers. In view of layered vdW heterostructure study and the recent progress of its photocatalysis application, this work will be of great interest and will promote the relevant theoretical and experimental efforts for seeking more efficient photocatalytic materials.

Acknowledgements

This work was supported by NSF of China Grant (21373113, 21403111, 21573254), Fundamental Research Funds for the Central Universities (30920140111008, 30920140132037), Jiangsu Province Science Foundation for Youths (BK2012394, BK20140526), China Postdoctoral Science Foundation funded project with Grant No. 2014M561576, and the Youth Innovation Promotion Association of the Chinese Academy of Sciences.

Notes and references

1 Y. Zheng, L. H. Lin, B. Wang and X. C. Wang, *Angew. Chem. Int. Ed.*, 2015, **54**, 12868-12884.
2 J. Liu, Y. Liu, N. Y. Liu, Y. Z. Han, X. Zhang, H. Huang, Y. Lifshitz, S. T. Lee, J. Zhong and Z. H. Kang, *Science*, 2015, **347**, 970-974.
3 X. C. Wang, K. Maeda, A. Thomas, K. Takanabe, G. Xin, J. M. Carlsson, K. Domen and M. Antonietti, *Nat. Mater.*, 2009, **8**, 76-80.
4 X. C. Miao, S. Tongay, M. K. Petterson, K. Berke, A. G. Rinzler, B. R. Appleton and A. F. Hebard, *Nano. Lett.*, 2012, **12**, 2745-2750.
5 L. W. Ji, M. Rao, H. M. Zheng, L. Zhang, Y. C. Li, W. H. Duan, J. H. Guo, E. J. Cairns and Y. G. Zhang, *J. Am. Chem. Soc.*, 2011, **133**, 18522-18525.
6 L. H. Hu, F. Y. Wu, C. T. Lin, A. N. Khlobystov and L. J. Li, *Nat. Commun.*, 2013, **4**, 1687.
7 J. Xiao, D. H. Mei, X. L. Li, W. Xu, D. Y. Wang, G. L. Graff, W. D. Bennett, Z. M. Nie, L. V. Saraf, I. A. Aksay, J. Liu and J. G. Zhang, *Nano Lett.*, 2011, **11**, 5071-5078.
8 Y. W. Zhu, S. Murali, M. D. Stoller, K. J. Ganesh, W. W. Cai, P. J. Ferreira, A. Pirkle, R. M. Wallace, K. A. Cychosz, M. Thommes, D. Su, E. A. Stach and R. S. Ruoff, *Science*, 2011, **332**, 1537-1541.
9 C. G. Liu, Z. N. Yu, D. Neff, A. Zhamu and B. Z. Jang, *Nano Lett.* 2010, **10**, 4863-4868.
10 Y. Wang, Z. Q. Shi, Y. Huang, Y. F. Ma, C. Y. Wang, M. M. Chen and Y. S. Chen, *J. Phys. Chem. C*, 2009, **113**, 13103-13107.
11 H. B. Heersche, P. Jarillo-Herrero, J. B. Oostinga, L. M. K. Vandersypen and A. F. Morpurgo, *Nature* 2007, **446**, 56-59.
12 G. Profeta, M. Calandra and F. Mauri, *Nat. Phys.*, 2012, **8**, 131-134.
13 C. N. Rao, A. K. Sood, K. S. Subrahmanyam and A. Govindaraj, *Angew. Chem. Int. Ed.*, 2009, **48**, 7752-7777.
14 J. S. Zhang, Y. Chen and X. C. Wang, *Energy Environ. Sci.*, 2015, **8**, 3092-3108.
15 S. Z. Butler, S. M. Hollen, L. Y. Cao, Y. Cui, J. A. Gupta, H. R. Gutierrez, T. F. Heinz, S. S. Hong, J. X. Huang, A. F. Ismach, E. Johnston-Halperin, M. Kuno, V. V. Plashnitsa, R. D. Robinson, R. S. Ruoff, S. Salahuddin, J. Shan, L. Shi, M. G. Spencer, M. Terrones, W. Windl and J. E. Goldberger, *ACS Nano*, 2013, **7**, 2898-2926.
16 A. Gupta, T. Sakthivel and S. Seal, *Prog. Mater. Sci.*, 2015, **73**, 44-126.
17 K. N. Duerloo, M. T. Ong and E. J. Reed, *J. Phys. Chem. Lett.*, 2012, **3**, 2871-2876.
18 M. S. Xu, T. Liang, M. M. Shi and H. Z. Chen, *Chem. Rev.* 2013, **113,** 3766-3798.
19 K. Varoon, X. Zhang, B. Elyassi, D. D. Brewer, M. Gettel, S. Kumar, J. A. Lee, S. Maheshwari, A. Mittal, C. Y. Sung, M. Cococcioni, L. F. Francis, A. V. McCormick, K. A. Mkhoyan and M. Tsapatsis, *Science*, 2011, **334**, 72-75.
20 J. N. Coleman, M. Lotya, A. O'Neill, S. D. Bergin, P. J. King, U. Khan, K. Young, A. Gaucher, S. De, R. J.Smith, I. V. Shvets, S. K. Arora, G. Stanton, H. Y. Kim, K. Lee, G. T. Kim, G. S. Duesberg, T. Hallam, J. J. Boland, J. J. Wang, J. F. Donegan, J. C. Grunlan, G. Moriarty, A. Shmeliov, R. J. Nicholls, J. M. Perkins, E. M. Grieveson, K. Theuwissen, D. W. McComb, P. D. Nellist and V. Nicolosi, *Science*, 2011, **331**, 568-571.

21 J. T. Jang, S. Jeong, J. W. Seo, M. C. Kim, E. Sim, Y. Oh, S. Nam, B. Park and J. Cheon, *J. Am. Chem. Soc.* 2011, **133**, 7636-7639.
22 Xu, M. Han, L. Dong and S. J. *ACS Appl. Mater. Inter.*, 2013, **5**, 12533.
23 A. J. Du, Z. H. Zhu and S. C. Smith, *J. Am. Chem. Soc.*, 2010, **132**, 2876-2877.
24 R. F. Lu, F. Li, J. Salafranca, E. J. Kan, C. Y. Xiao and K. M. Deng, *Phys. Chem. Chem. Phys.*, 2014, **16**, 4299-4304.
25 Q. Li, B. D. Guo, J. G. Yu, J. G. Ran, B. H. Zhang, H. J. Yan and J. R.Gong, *J, Am. Chem. Soc.*, 2011, **133**, 10878-10884.
26 G. G. Zhang, M. G. Zhang, X. X. Ye, X. Q. Qiu, S. Lin and X. C. Wang, *Adv. Mater.*, 2014, **26**, 805-809.
27 J. J. Xue, S. S. Ma, Y. M. Zhou, Z. W. Zhang and M. He, *ACS Appl. Mater. Inter.*, 2015, **7**, 9630-9637.
28 A. K. Geim and I. V. Grigorieva, *Nature*, 2013, **499**, 419-425.
29 C. R. Dean, A. F. Young, I. Meric, C. Lee, L. Wang, S. Sorgenfrei, K. Watanabe, T. Taniguchi, P. Kim, K. L. Shepard and J. Hone, *Nat. Nanotech.*, 2010, **5**, 722-726.
30 A. J. Du, S. Sanvito, Z. Li, D. W. Wang, Y. Jiao, T. Liao, Q. Sun, Y. H. Ng, Z. H. Zhu, R. Amal and S. C. Smith, *J. Am. Chem. Soc.*, 2012, **134**, 4393-4397.
31 X. P. Hong, J. Kim, S. F. Shi, Y. Zhang, C. H. Jin, Y. H. Sun, S. Tongay, J. Q. Wu, Y. F. Zhang and F. Wang, *Nat Nanotech.*, 2014, **9**, 682-686.
32 J. Yang, D. Voiry, S. J. Ahn, D. Kang, A. Y. Kim and M. Chhowalla and H. S. Shin, *Angew. Chem. Int. Ed.*, 2013, **52**, 13751-13754.
33 M. L. Tsai, S. H. Su, J. K. Chang, D. S. Tsai, C. H. Chen, C. I. Wu, L. J. Li, L. J. Chen and J. H. He, *ACS Nano*, 2014, **8**, 8317-8322.
34 L. Li, X. S. Fang, T. Y. Zhai, M. Y. Liao, U. K. Gautam, X. C. Wu, Y. Koide, Y. Bando and D. Golberg, *Adv. Mater.*, 2010, **22**, 4151-4156.
35 L. Li, H. Q. Wang, X. S. Fang, T. Y. Zhai, Y. Bando and D. Golberg, *Energy Environ. Sci.*, 2011, **4**, 2586-2590.
36 Z. Y. Zeng, Z. Y. Yin, X. Huang, H. Li, Q. Y. He, G. Lu, F. Boey and H. Zhang, *Angew. Chem. Int. Ed.*, 2011, **50**, 11093-11097.
37 M. Zhang, Y. M. Zhu, X. S. Wang, Q. L. Feng, S. Qiao, W. Wen, Y. F. Chen, M. H. Cui, J. Zhang, C. Cai and L. M. Xie, *J. Am. Chem. Soc.*, 2015. **137**, 7051-7054.
38 S. Jeong, D. Yoo, M. Ahn, P. Miro, T. Heine and J. Cheon, *Nat. Commun.*, 2015, **6**, 5763.
39 H. L. Zhuang and R. G. Hennig, *J. Phys. Chem. C*, 2013, **117**, 20440-20445.
40 Y. Li, J. Kang and J. B. Li, *RSC Adv.*, 2014, **4**, 7396-7401.
41 M. Corso, W. Auwarter, M. Muntwiler, A. Tamai, T. Greber and J. Osterwalder, *Science*, 2004, **303**, 217-220.
42 A. Y. Liu, R. M. Wentzcovitch and M. L. Cohen, *Phys. Rev. B*, 1989, **39**, 1760-1765.
43 G. Kresse and J. Furthmüller, *Phys. Rev. B*, 1996, **385**, 11169-11186.
44 P. John and M. Perdew Kieron Burke Ernzerhof, *Phys. Rev. Lett.*, 1996, **77**, 3865-3868.
45 G. Kresse and J. Furthmuller, *Comput. Mater. Sci.*, 1996, **6**, 15-619.
46 S. Grimme, *J. Comput. Chem.*, 2006, **27**, 1787-1799.
47 J. Heyd, G. E. Scuseria and M.Ernzerhof, *J. Chem. Phys.*, 2003, **118**, 8207.
48 H. Jiang, *J. Chem. Phys.*, 2011, **134,** 204705.
49 F. Guinea and T. Low, *Philos. Trans. R. Soc. London A: Math., Phys. Eng. Sci.*, 2010, **368**, 5391-5402.
50 W. X. Zhang, Z. S. Huang, W. L. Zhang and Y. R. Li, *Nano Res.*, 2014, **7**, 1731-1737.
51 X. Du, I. Skachko, A. Barker and E. Y. Andrei, *Nat. Nanotech.*, 2008, **3**, 491-495.
52 N. Kerszberg and P. Suryanarayana, *RSC Adv.*, 2015, **5**, 43810-43814.
53 W. Hu and J. L. Yang, arXiv:1411.0357 (cond-mat.mtrl-sci) 2015.
54 K. S. Novoselov, D. Jiang, F. Schedin, T. J. Booth, V. V. Khotkevich, S. V. Morozov and A. K. Geim, *Proc. Natl. Acad. Sci. U.S.A.*, 2005, **102**, 10451-10453.
55 J. V. Liebig, *Ann. Pharm.*, 1834, **10**, 10.
56 Y. Wang, X. C. Wang and M. Antonietti, *Angew. Chem. Int. Ed.*, 2012, **51**, 68-89.
57 Y. Zheng, Y. Jiao, J. Chen, J. Liu, J. Liang, A. J. Du, W. M. Zhang, Z. H. Zhu, S. C. Smith, M. Jaroniec, G. Q. Lu and S. Z. Qiao, *J. Am. Chem. Soc.*, 2011, **133**, 20116-20119.
58 S. W. Cao and J. G. Yu, *J. Phys. Chem. Lett.*, 2014, **5**, 2101-2107.
59 X. R. Li, Y. Dai, Y. D. Ma, S. H. Han and B. B. Huang, *Phys. Chem. Chem. Phys.*, 2014, **16**, 4230-4235.
60 Y. Y. Liang, Y. G. Li, H. L. Wang and H. Dai, *J. Am. Chem. Soc.*, 2013, **135**, 2013-2036.
61 Y. D. Hou, A. B. Laursen, J. H. Zhang, G. G. Zhang, Y. S. Zhu, X. C. Wang, S. Dahl and I. Chorkendorff, *Angew. Chem. Int. Ed.*, 2013, **52**, 3621-3625.
62 X. C. Wang, S. Blechert and M. Antonietti, *ACS Catal.*, 2012, **2**, 1596-1606.
63 X. P. Wang, L. X. Wang, F. Zhao, C. G. Hu, Y. Zhao, Z. P. Zhang, S. L. Chen and G. Q. Shi, L. T. Qu, *Nanoscale*, 2015, **7**, 3035-3042.
64 X. Huang, C. L. Tan, Z. Y. Yin and H. Zhang, *Adv. Mater.*, 2014, **26**, 2185-2204.
65 J. J. Wang, Z. Y. Guan, J. Huang, Q. X. Li and J. L. Yang, *J. Mater. Chem. A*, 2014, **2**, 7960-7966.
66 K. Goto, I. Rozhanskii, Y. Yamakawa, T. Otsuki and Y. Naito, *Polym. J.*, 2008, **41**, 95-104.
67 C. H. Fujimoto, M. A. Hickner, C. J. Cornelius and D. A. Loy, *Macromolecules*, 2005, **38**, 5010-5016.
68 H. L. Du, J. Y. Li, J. Zhang, G. Su, X. Y. Li and Y. L. Zhao, *J. Phys. Chem. C*, 2011, **115**, 23261-23266.
69 S. Jungthawan, P. Reunchan and S. Limpijumnong, *Carbon*, 2013, **54**, 359-364.
70 C. J. Huang, C. Chen, M. W. Zhang, L. H. Lin, X. X. Ye, S. Lin, M. Antonietti and X. C.Wang, *Nat. Commun.*, 2015, **6**, 7698.

Table of Content

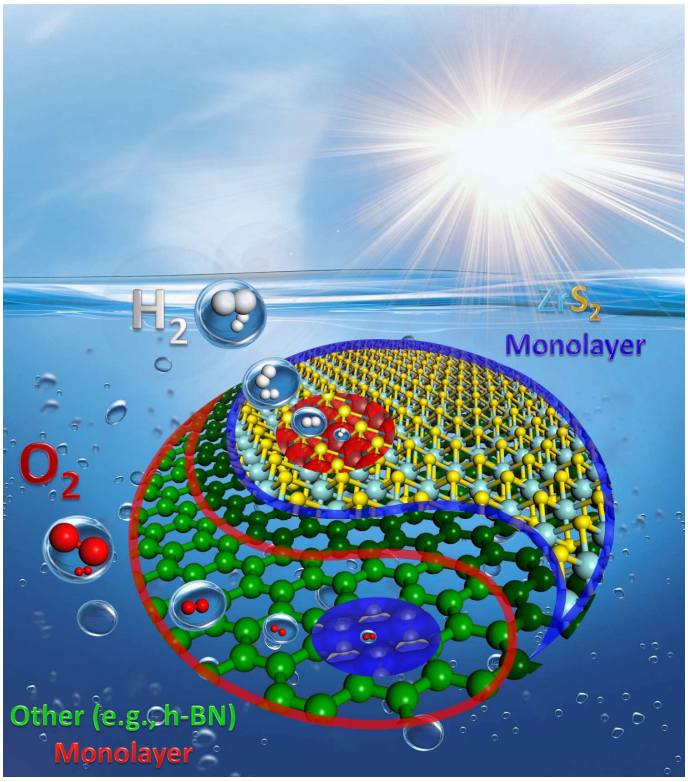

Bilayer ZrS_2-based vdW heterostructures are proposed as efficient photo-catalysts for water splitting under visible light.

Broader context

In recent decade, utilization of solar energy and hydrogen energy has attracted much attention both in industrial and scientific research fields. It is highly demanded to develop novel environmental-friendly energy materials for solar energy harvesting and solar energy conversion via water splitting. For this purpose, we designed several vdW heterostructures using metal-free 2D sustainable materials to couple with ZrS_2 nanosheet. Since most of the solar energy comes from the visible-light region, to enhance the quantum efficiency, the absorption peak of photoresponse materials should be located within the range from 400 nm to 760 nm. Our results show good visible light response and efficient charge separation in proposed graphene/ZrS_2, h-BN/ZrS_2, g-C_3N_4/ZrS_2, and polyphenylene/ZrS_2 heterostructures. Particularly for h-BN/ZrS_2 and g-C_3N_4/ZrS_2, suitable CBM and VBM positions with enough driving forces for electron and hole transfer have also been accomplished by applying slight stain. Although semiconductor heterostructures have been intensively investigated in solar photocatalysis, the layered junctions of 2D crystals via strain to tune the band structure, charge separation and visible light absorption are much less reported, and the vdW heterostructures in this work could be envisaged to emerge as a new type of semiconductor for solar energy applications.